Theory of acoustic scattering by supported ridges at a solid-liquid interface

A. Khelif,[1] J. O. Vasseur,[2] Ph. Lambin,[1] B. Djafari-Rouhani,[2] and P. A. Deymier[3]
[1]*Laboratoire de Physique du Solide, Département de Physique, Facultés Notre-Dame de la Paix, 5000 Namur, Belgium*
[2]*Laboratoire de Dynamique et Structures des Matériaux Moléculaires, UPRESA CNRS 8024, UFR de Physique, Université de Lille I, 59655 Villeneuve d'Ascq Cédex, France*
[3]*Department of Materials Science and Engineering, University of Arizona, Tucson, Arizona 85721*
(Received 10 July 2001; published 7 February 2002)

We combine a general Green's function formalism and an approach due to Nyborg [W. L. Nyborg, in *Acoustic Streaming, Physical Acoustics*, edited by W. P. Mason (Academic, London, 1965), Vol. II B, Chap. 11] to calculate the first-order pressure and second-order pressure gradient fields in the vicinity of solid inhomogeneities at a solid/liquid interface. We treat the problem of scattering of an incident acoustic plane wave by a single ridge and two parallel ridges separated by a trench on a planar substrate. The calculated vibrational density of states shows the existence of resonances at low frequencies, especially in the case of a trench. Excitation of a trench resonant vibrational mode enhances the magnitude of the first-order pressure and of the second-order pressure gradient. The resonant frequencies of a trench decrease and the pressure enhancement increases with increasing aspect ratio of the ridges (height to width).

DOI: 10.1103/PhysRevE.65.036601 PACS number(s): 43.25.+y, 62.60.+v, 68.08.−p

I. INTRODUCTION

The problem of the interaction between acoustic waves and solid surfaces in contact with fluids has relevance to the electronic industry. For instance, megasonic waves are extensively used to remove contaminant particles from planar and patterned silicon wafers immersed in a water-based solution during processing of integrated circuits [1].

In a previous study, we employed a method based on a Green's function formalism to solve the linear wave equation, to calculate the acoustic pressure field around an infinite ridge on a silicon wafer immersed in water subjected to a megasonic beam [2]. This study showed that the acoustic shear stress on a ridge has no detrimental effect on the integrity of patterned silicon wafers. We then implemented a methodology for determining the time-independent second-order solution to the nonlinear Navier-Stokes equation [3]. This approach was used to calculate the second-order streaming force in a viscous fluid in the vicinity of a planar silicon/water interface. Schlichting streaming or acoustic streaming in a narrow boundary layer was identified as a potential mechanism for megasonic cleaning of silicon wafers [4]. In the present paper, we combine the Green's function formalism for nonplanar solid/fluid interfaces of Ref. [2] and the methodology for solving the nonlinear effects of Ref. [3] to shed light on the first-order (linear) and second-order (nonlinear) pressure field in the vicinity of surface inhomogeneities on a solid substrate in contact with a fluid. We focus on a single infinite ridge and two adjacent parallel ridges separated by a trench. We pay particular attention to conditions associated with resonances for which variations in the first-order and second-order pressure fields are most significant. Our paper builds on previous studies of acoustic resonances of a protuberance or indentation on an elastic solid medium [5,6] but focuses on resonances of fluid features. The relevance of these resonant conditions to acoustic wave-based cleaning technologies used in the electronic industry are discussed in the conclusion. The formulation of the theoretical methods for calculating linear and nonlinear solutions to the acoustic wave equation is presented in some details in Sec. II. The calculated vibrational density of states, first-order pressure, and second-order pressure gradient for several geometries of the surface inhomogeneities are reported in Sec. III.

II. FORMULATION

A. Geometry

In this paper, we consider two inhomogeneous systems, composed of a rigid solid and a nonviscous fluid. These systems model rough interfaces with an infinite ridge and an infinite trench composed of two parallel ridges, respectively. In the two cases the substrate fills the half space $X_3<0$ in the Cartesian coordinate system (O,X_1,X_2,X_3). The axis of the ridges is oriented parallel to the X_2 direction. In this study, we assume that the ridge has a cross section with an exponential shape [see Fig. 1(a)] defined in the (X_1,O,X_3) plane by

$$X_3=f(X_1)=A\exp\left[-\left(\frac{X_1}{R}\right)^4\right]. \tag{1}$$

We obtain a trench by constructing two exponential ridges [see Fig. 1(b)]. The cross section of the trench (double ridge) is given by

$$X_3=f(X_1)=A\exp\left[-\left(\frac{|X_1|}{R}-1.5\right)^4\right]+0.02\left(-2\frac{|X_1|}{R}+6\right)$$
$$\text{with}\quad -3\leqslant\frac{X_1}{R}\leqslant+3. \tag{2}$$

The linear term in the previous expression is added to the exponential function in order to elevate slightly the bottom of the trench with respect to the planar interface. In the preceding expressions, A controls the height of the ridge and R

its width. We define the geometric aspect ratio by $A/2R$. The geometries expressed in Eqs. (1) and (2) attempt to model patterned silicon wafers encountered in integrated circuits although we have chosen the exponential shape for the sake of mathematical practicality. The fourth power in the exponential argument is chosen to mimick the nearly rectangular cross section of ridges in integrated circuits.

B. Nonlinear and linear acoustic fields

The nonlinear motion in a viscous fluid, in absence of external forces, is governed by Navier-Stokes equation

$$\rho\left[\frac{\partial \mathbf{v}}{\partial t}+(\mathbf{v}\cdot\boldsymbol{\nabla})\mathbf{v}\right]=-\boldsymbol{\nabla}p+\mu\nabla^2\mathbf{v}+\left(\mu'+\frac{\mu}{3}\right)\boldsymbol{\nabla}(\boldsymbol{\nabla}\cdot\mathbf{v}), \tag{3}$$

where $\mathbf{v}$ is the velocity, ρ the density, μ and μ' the coefficients of shear and dilatation viscosity, and p the pressure. Since in this paper, for the sake of simplicity, we treat the case of nonviscous fluids. Navier-Stokes equation reduces to the nonlinear Euler equation. We briefly recall in this section the method used for determining the time-independent second-order solution to the nonlinear Euler equation. Following Nyborg's approach [7], one makes the approximation that the fluid velocity, the excess pressure, and the excess density are written as the superpositions

$$\mathbf{v}=\mathbf{v}^{(1)}+\mathbf{v}^{(2)}, \tag{4}$$

$$p-p^{(0)}=p^{(1)}+p^{(2)}, \tag{5}$$

$$\rho-\rho^{(0)}=\rho^{(1)}+\rho^{(2)}. \tag{6}$$

Here, the terms $p^{(0)}$ and $\rho^{(0)}$ are the static pressure and the density of the fluid in absence of acoustic field and are time and space independent. $\mathbf{v}^{(1)}$, $p^{(1)}$, and $\rho^{(1)}$ are first-order approximations to the nonlinear problem. These quantities follow harmonic motions with a time dependence $e^{-i\omega t}$ where ω is the pulsation. The second-order terms, $\mathbf{v}^{(2)}$, $p^{(2)}$, and $\rho^{(2)}$ are time independent.

Inserting Eqs. (4), (5), and (6) into the nonlinear Euler equation, eliminating all terms of order greater than two, averaging the remaining terms over several sonic cycles and grouping the terms of the same order, yields the following equations:

$$\boldsymbol{\nabla}p^{(1)}=-\rho^{(0)}\frac{\partial \mathbf{v}^{(1)}}{\partial t}, \tag{7}$$

$$\boldsymbol{\nabla}p^{(2)}\equiv-\rho^{(0)}\langle(\mathbf{v}^{(1)}\cdot\boldsymbol{\nabla})\mathbf{v}^{(1)}+\mathbf{v}^{(1)}(\boldsymbol{\nabla}\cdot\mathbf{v}^{(1)})\rangle. \tag{8}$$

Equation (7) is formally equivalent to the equation of propagation of longitudinal waves in a nonviscous fluid. Equation (8) gives the second-order pressure gradient in terms of first-order velocity field. The brackets $\langle\,\rangle$ indicate that a time average is taken over several sonic cycles in order to retain only these terms that are time independent. In Nyborg's approach, for nonviscous fluids, $\boldsymbol{\nabla}p^{(2)}$ represents a volumic force directly relevant to the problem of acoustic cleaning [3,7]. A contaminant particle adhering to the surface of a wafer may be removed provided this volumic force counteracts the adhesion force of this particle to the surface.

Since the fluid undergoes harmonic motion and considering complex notation, (i.e., $\mathbf{v}^{(1)}=\mathrm{Re}\{\tilde{\mathbf{v}}^{(1)}\}$), the first-order velocity field is

$$\tilde{\mathbf{v}}^{(1)}=\frac{-i}{\omega\rho^{(0)}}\boldsymbol{\nabla}\tilde{p}^{(1)}. \tag{9}$$

With this, Eq. (8) may be written in complex notation as

$$\boldsymbol{\nabla}p^{(2)}=-\rho^{(0)}\tfrac{1}{2}\mathrm{Re}\begin{pmatrix} 2\tilde{v}_1^{(1)}\dfrac{\partial\tilde{v}_1^{(1)*}}{\partial X_1}+\tilde{v}_3^{(1)}\dfrac{\partial\tilde{v}_1^{(1)*}}{\partial X_3}+\tilde{v}_1^{(1)}\dfrac{\partial\tilde{v}_3^{(1)*}}{\partial X_3} \\ 2\tilde{v}_3^{(1)}\dfrac{\partial\tilde{v}_3^{(1)*}}{\partial X_3}+\tilde{v}_3^{(1)}\dfrac{\partial\tilde{v}_1^{(1)*}}{\partial X_1}+\tilde{v}_1^{(1)}\dfrac{\partial\tilde{v}_3^{(1)*}}{\partial X_1} \end{pmatrix}, \tag{10}$$

where the superscript * stands for the complex conjugate quantity. This equation enables us to calculate second-order corrections to the acoustic pressure field from solutions to the linear acoustic wave equation.

In the limit of a fluid, such as water, with very low compressibility, ρ is assimilated to $\rho^{(0)}$. Assuming that the longitudinal speed of sound in the fluid, c_l, is constant, taking

$$\tilde{p}^{(1)}=i\rho^{(0)}c_l^2\omega\boldsymbol{\nabla}\cdot\tilde{\mathbf{v}}^{(1)}, \tag{11}$$

and in the case of irrotational motion of the fluid, Eq. (7) becomes

$$\Delta\tilde{p}^{(1)}-\frac{1}{c_l^2}\frac{\partial^2\tilde{p}^{(1)}}{\partial t^2}=\Delta\tilde{p}^{(1)}+\frac{\omega^2}{c_l^2}\tilde{p}^{(1)}=0. \tag{12}$$

This equation is recast in the form

$$\frac{1}{\rho^{(0)}}\left(\frac{\partial^2}{\partial X_1^2}+\frac{\partial^2}{\partial X_3^2}+\frac{\omega^2}{c_l^2}\right)\tilde{p}^{(1)}(X_1,X_3)=0. \tag{13}$$

Since the solid is rigid, we must, therefore, solve Eq. (13) for the liquid motion subject to the boundary condition $\boldsymbol{\nabla}\tilde{p}^{(1)}=0$ in the direction normal to the solid-liquid interface. For this we employ a method based on Green's functions [8].

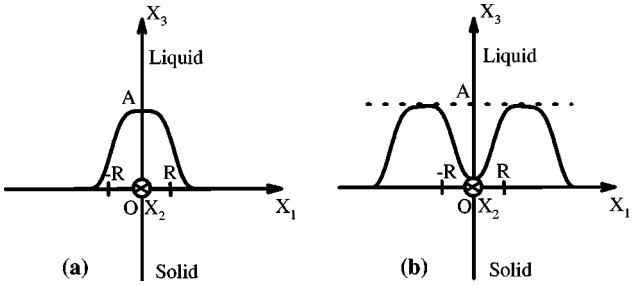

FIG. 1. Cross section of (a) a single exponential ridge and (b) two exponential ridges separated by a trench (thick line). *A* and *R* measure the height and width of the inhomogeneity.

Equation (13) may be written in the form, $H\tilde{p}^{(1)}=0$, where the differential operator H is defined as

$$H=\frac{1}{\rho^{(0)}}\left(\frac{\partial^2}{\partial X_1^2}+\frac{\partial^2}{\partial X_3^2}+\frac{\omega^2}{c_l^2}\right). \tag{14}$$

The Green's function $G(X_1,X_3;X_1',X_3'|\omega)$ is the solution of an equation similar to Eq. (13), namely,

$$\frac{1}{\rho^{(0)}}\left(\frac{\partial^2}{\partial X_1^2}+\frac{\partial^2}{\partial X_3^2}+\frac{\omega^2}{c_l^2}\right)G(X_1,X_3;X_1',X_3'|\omega)$$
$$=\delta(X_1-X_1')\,\delta(X_3-X_3') \tag{15}$$

with again the appropriate boundary conditions. Analytical solutions of Eq. (15) are known in the following two cases: an unbounded fluid and a fluid bounded by a planar rigid surface. The Green's function G^{∞} of an infinite unbounded fluid is given by

$$G^{\infty}(X_1,X_3;X_1',X_3'|\omega)=-\frac{i\rho^{(0)}}{4}H_0^{(1)}\left\{\frac{\omega}{c_l}[(X_2-X_1')^2+(X_3-X_3')^2]^{1/2}\right\}, \tag{16}$$

where $H_0^{(1)}$ is a Hankel function of the first kind. The Green's function g_b for the semi-infinite fluid bounded by a rigid planar surface at $X_3=0$, is also known and takes the form

$$g_b(X_1,X_3;X_1',X_3'|\omega)$$
$$=-\frac{i\rho^{(0)}}{4}\left\{H_0^{(1)}\left(\frac{\omega}{c_l}[(X_1-X_1')^2+(X_3-X_3')^2]^{1/2}\right)+H_0^{(1)}\left(\frac{\omega}{c_l}[(X_1-X_1')^2+(X_3+X_3')^2]^{1/2}\right)\right\}. \tag{17}$$

The Green's function for the fluid in contact with a rigid planar solid supporting a rigid raised inhomogeneity (e.g., ridge) is not known analytically but it can be constructed mathematically by cutting out of the semi-infinite fluid the volume occupied by the inhomogeneity (Fig. 1) and applying the boundary condition on that additional interface. This mathematical operation is achieved by the application of a cleavage operator V onto g_b. The cleavage operator is defined as $(1/\rho^{(0)})(\partial/\partial_{\mathbf{n}})$, where $(\partial/\partial_{\mathbf{n}})$ means the normal derivative at the boundaries. The cleavage operator is, therefore, only operating in the space M of the interface being cut. Here M represents the surface of the raised inhomogeneity. We obtain the Green's function g_f of the fluid in which one has made a cut from the relation [8],

$$g_f(M,M)[I(M,M)+V(M,M)g_b(M,M)]=g_b(M,M), \tag{18}$$

where $I(M,M)$ is the unit matrix. Equation (18) is an integral equation, with integration over the solid/fluid interface space M. Once the interface elements of g_f are known in the space M, we can deduce the Green's function in the space D encompassing the entire fluid via

$$g_f(D,D)=g_b(D,D)+g_b(D,M)[g_b^{-1}(M,M)g_f(M,M)-I(M,M)]g_b^{-1}(M,M)g_b(M,D). \tag{19}$$

The first term on the right-hand side of Eq. (19) is the Green's function of the fluid bounded by a planar interface. The second term represents a correction to the Green's function of the fluid with a planar interface that accounts for the presence of the raised inhomogeneity. This term arises from scattering of the acoustic waves by the inhomogeneity. From Eq. (19) it is convenient to define a scattering function $T(M,M)$ as the expression

$$T(M,M)=[g_b^{-1}(M,M)g_f(M,M)-I(M,M)]g_b^{-1}(M,M). \tag{20}$$

Then, by analogy with Eq. (19), the linear pressure field $\tilde{p}^{(1)}(D)$ in the fluid bounded by a surface supporting an inhomogeneity can be written in the form

$$\tilde{p}^{(1)}(D)=\tilde{P}(D)+g_b(D,M)T(M,M)\tilde{P}(M). \tag{21}$$

From a pratical point of view, we consider the case of an incident compression wave of pulsation ω traveling towards the surface with an incident angle θ,

$$\tilde{p}^{\infty}(X_1,X_3|\omega)=\frac{W}{2}\exp\left[\frac{i\omega}{c_l}(X_1\sin\theta-X_3\cos\theta)\right], \tag{22}$$

where $W/2$ is the amplitude of the compression wave. In the absence of an inhomogeneity, the acoustic wave is solely reflected by the rigid planar surface. The linear pressure field $\tilde{P}(D)$ in the semi-infinite liquid bounded by a planar surface takes the following representation:

$$\tilde{P}(X_1,X_3|\omega)=\frac{W}{2}\left\{\exp\left[\frac{i\omega}{c_l}(X_1\sin\theta-X_3\cos\theta)\right]+\exp\left[\frac{i\omega}{c_l}(X_1\sin\theta+X_3\cos\theta)\right]\right\}, \tag{23}$$

where the second term gives the compression wave reflected from the perfect planar surface.

C. Density of states

The density of states (DOS) inside the fluid, can be calculated from the Green's function of the solid/fluid system with a surface inhomogeneity g_f [9]. Here we report the variation of the total density of states due to the presence of the inhomogeneity onto the planar surface. It is defined by

$$\Delta n(\omega) = \frac{1}{\pi}\frac{d}{d\omega}\{\arg[\det(g_f^{-1}(M,M))] - \arg[\det(g_b^{-1}(M,M))]\}. \quad (24)$$

Owing to the symmetry of the geometry, the Green's function may be separated into its symmetric and antisymmetric parts allowing for the calculations of the contributions of the symmetric and antisymmetric vibrational modes to the density of states.

D. Practical implementation

In order to obtain the scattering function $T(M,M)$ and the first-order pressure field $p^{(1)}(D)$, one solves numerically the integral Eqs. (18), (20), and (21). For this, we discretize space that transforms these equations into discrete matrix relations. For this purpose, the axis X_1 is divided into $2N$ intervals having their middle at the points X_n such that $X_n = (n+1/2)\Delta X$ with $n=-N, -N+1, \ldots, N-1$ and $\Delta X = R/N$. In this way, the continuous curve delimiting the interfacial space M is divided into small segments. The discretization of the interface domain for the ridge and the trench (dual ridges) is done with $N=300$ and $N=500$ in order to have a good balance between convergence and computation time. The matrix $g_f(M,M)$, is then calculated from known matrices using Eq. (18). It is then inserted into Eq. (10) to obtain the scattering matrix $T(M,M)$, which in turns is used into Eq. (21) to determine the first-order pressure field in the fluid. Further details of the calculation as well as the numerical procedure are given in Refs. [10] and [11]. The gradient of the second-order pressure is obtained from first- and second-order derivatives of the first-order pressure. All derivatives in the computational method are calculated with a finite difference method.

III. RESULTS

A. Density of states

Figure 2 displays the variation of the total density of states $\Delta n(\omega)$ due to the presence of the ridge or the trench onto the planar surface as function of the reduced frequency $\omega^* = \omega R/c_l$. In panels (a) and (b), these DOS are calculated for a single ridge with two heights $A=2R$ and $A=4R$. The same aspect ratios are considered for the trench (double ridge) in panels (c) and (d). The variation in density of states exhibits for all graphs an overall decrease in the background with increasing reduced frequency. This reduction in density of states can be understood by considering a fixed frequency and a variable ridge size R. Indeed at constant frequency, an increasing reduced frequency, is only due to a loss of matter in the fluid and, therefore, a loss in the number of vibrational

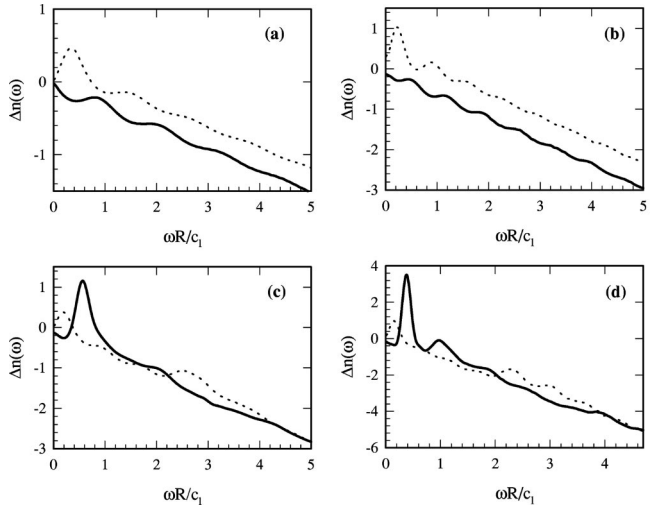

FIG. 2. Variation in density of states as a function of reduced frequency $\omega^* = \omega R/c_l$ for a single ridge with (a) $A=2R$, (b) $A=4R$, and a trench (dual ridges) for (c) $A=2R$ and (d) $A=4R$. The solid lines and the dashed lines are for symmetric and antisymmetric vibrational modes, respectively.

states. Acoustic resonances appear in these figures as peaks in the variation of the DOS. The most pronounced resonances occur at relatively low reduced frequencies. The observed resonances are associated with vibrations in the fluid. In the case of a patterned silicon wafer immersed in water, the assumption of rigidity of the solid substrate is justified because of the strong contrast between the density and elastic constants of silicon and water. Nevertheless this assumption when lifted should only affect the DOS spectrum by introducing additional resonant peaks at high frequency owing to the larger speed of sound in a solid compared to a fluid. These additional resonances would result from vibrations in the elastic solid ridges. In fact, it has been shown [9,11] that the first resonance state of a solid ridge supported by a solid substrate occurs at a reduced frequency $\omega R/c^s{}_t \approx 1$ where $c^s{}_t$ is the transverse speed of sound in the solid ridge. In the case of a patterned silicon wafer immersed in water, this corresponds to a reduced frequency $\omega R/c_l \approx 4$ very much larger than those considered in acoustic cleaning. For the single rigid ridge system, the antisymmetric modes are more important than the symmetric ones. For the trench this tendency is inverted with the dominant resonances associated with the symmetric modes. This may be explained by a coupling between the antisymmetric modes of the fluid around each ridge yielding an overall symmetric effect. The frequency of the resonances depends strongly on the aspect ratio of the surface inhomogeneities. For instance, the reduced frequency of the antisymmetric resonances for the single ridge decreases from a value of 0.33 to 0.22 as the height is doubled. Similarly, the reduced frequency of the predominant symmetric resonant modes associated with the trench drops from 0.56 to 0.38 upon doubling the height of its constitutive ridges. It is worthy noticing that the reduced frequency of the resonances nearly scales as the inverse of the square root of the inhomogeneity height. This observation is reminiscent of the characteristic frequencies of simple harmonic oscillators

scaling as the inverse of the square root of its mass. The amplitude of the resonant peak increases with increasing aspect ratio. This effect is more significant for a trench than for the ridge. Indeed, the problem of propagation of longitudinal waves in a nonviscous fluid bound by a rigid substrate with two rigid ridges is isomorphic to the problem of propagation of transverse waves in a semi-infinite elastic solid, bound by a vacuum, in which two trenches are cut. The elastic material separating the two trenches in that latter system is, therefore, equivalent to the trench filled with fluid that we study. This elastic material may be viewed as a single elastic ridge. It has been shown that an elastic ridge with an aspect ratio of 1:1 exhibits resonating vibrational modes near a reduced frequency of 0.5 [12]. The trench filled with liquid will, therefore, resonate at the same reduced frequency. The number of resonating modes increases with the depth of the trench.

B. Acoustic pressure

In this section, we report on the amplitude of the first-order acoustic pressure field in the vicinity of a trench (double ridge). Since the density of states at the resonant frequency of a trench is significantly higher than that of a single ridge, the effect on the pressure field is more pronounced for the former geometry. For instance, in the case of a single ridge with an aspect ratio 1:1, the first-order pressure field differs only slightly from the pressure field in a semi-infinite liquid, namely, a standing wave varying such as $\cos(\omega c_l/X_3)$ for a normal incident wave $\theta=0$. The first-order pressure field is only distorted in the vicinity of the ridge in order to satisfy the continuity condition of the displacement at the solid/liquid interface along the ridge surface.

In Fig. 3, we have investigated the effect of the trench aspect ratio and of the angle of incidence on the first-order pressure field at the lowest characteristic resonant frequency. The first-order pressure is reported in unit of the magnitude of the incident wave *W*. Figure 3 represents two-dimensional contour maps of the real part of the first-order pressure field with the lines representing isobars. In the case of a normal incidence [Figs. 3(a) and 3(b)], the pressure amplitude increases beyond the incident wave amplitude as one approaches the bottom of the trench, this being more significant for a deeper trench. The real part of the pressure exceeds that of the incident wave by up to a factor of 5 inside the deepest trench studied. Even higher pressure amplitudes can be attained inside the trench by changing the angle of the incident wave [see Fig. 3(c)] and an enhancement by a factor of 10 is observed at the bottom of the trench. This spectacular behavior is best seen by contrasting the resonant case [Fig. 3(c)] and the pressure field inside a trench under nonresonant conditions, at a reduced frequency of 0.2 [see Fig. 3(d)]. One also notes that the resonant frequencies and hence the acoustic pressure are very sensitive to the geometric ratio $A/2R$ of the inhomogeneity and slightly depends on its shape. Indeed the resonant states of the ridge were obtained at similar frequencies than those of a parabolic shape raised feature [9]. A different power of the exponential argument in Eqs. (1) and (2) only leads to sharper resonances in the DOS spectrum.

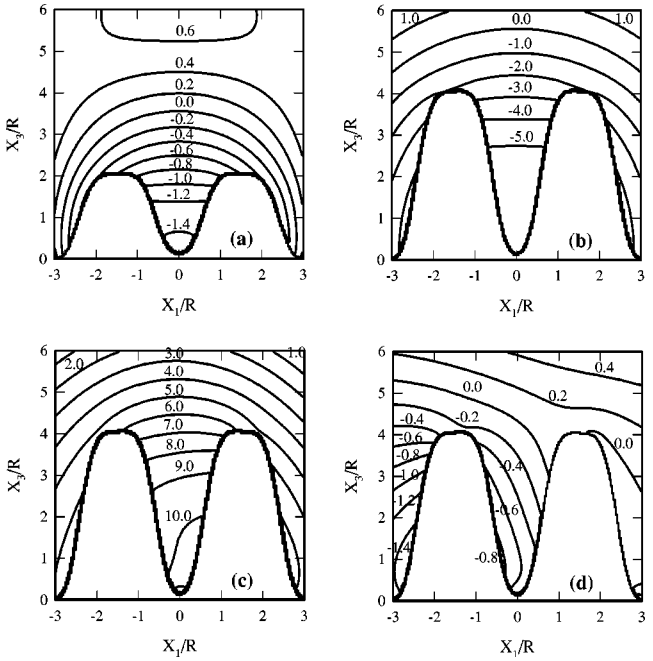

FIG. 3. First-order pressure fields around the dual ridges system (trench) for (a) $A=2R$, a normal incident wave ($\theta=0$), and at a reduced resonant frequency $\omega^*=0.56$; (b) $A=4R$, $\theta=0$, and at a reduced resonant frequency $\omega^*=0.38$; (c) $A=4R$, grazing incident wave ($\theta\approx 90°$), $\omega^*=0.38$; (d) $A=4R$, grazing incident wave ($\theta\approx 90°$), and at a nonresonant reduced frequency $\omega^*=0.2$. The labels on the isobars are in units of *W* (the pressure amplitude of the incident wave).

C. Gradient of second-order pressure

To obtain more manageable values for the second-order pressure gradient, we define a scaled pressure gradient $\nabla\hat{p}^{(2)}$ by $\nabla p^{(2)}=\nabla\hat{p}^{(2)}(C_l^2W^2/R)10^{-20}\,\mathrm{N\,m^{-3}}$. Figure 4 illustrates the spatial variations of the second-order pressure gradient in the two directions X_1 and X_3 for the trenches with aspect ratio 1:1 and 2:1 at the resonant frequency and normal incidence. The magnitude and direction of the components of the gradient are given as contour maps of $\mathrm{sgn}(\nabla_i\hat{p}^{(2)})\log_{10}(|\nabla_i\hat{p}^{(2)}|)$ with $i=1$, 3, and ∇_i representing the ith component of the ∇ operator. A negative sign indicates that the gradient is oriented along the direction of the negative X_1 axis. For a symmetric excitation (normal incident wave) the second-order pressure gradient $\nabla_1 p^{(2)}$ is an antisymmetrical function of X_1 while $\nabla_3 p^{(2)}$ is symmetrical. The extreme magnitude of the components of the second-order pressure gradient for the deep resonating trench is nearly one order of magnitude larger than that of the shallow trench. The components of the pressure gradients vary rapidly over very short distances and show complicated spatial patterns. These patterns are very sensitive to the angle the incident wave makes with the planar substrate but not the magnitude of the pressure gradient [see Fig. (5)]. In Fig. (5), we compare the second-order pressure gradient fields for a deep trench (aspect ratio 2:1) stimulated with a grazing wave under resonant and nonresonant conditions. It is clear that excitation of resonant modes raises the components, $\nabla_1 p^{(2)}$ and $\nabla_3 p^{(2)}$ by one order of magnitude in many locations.

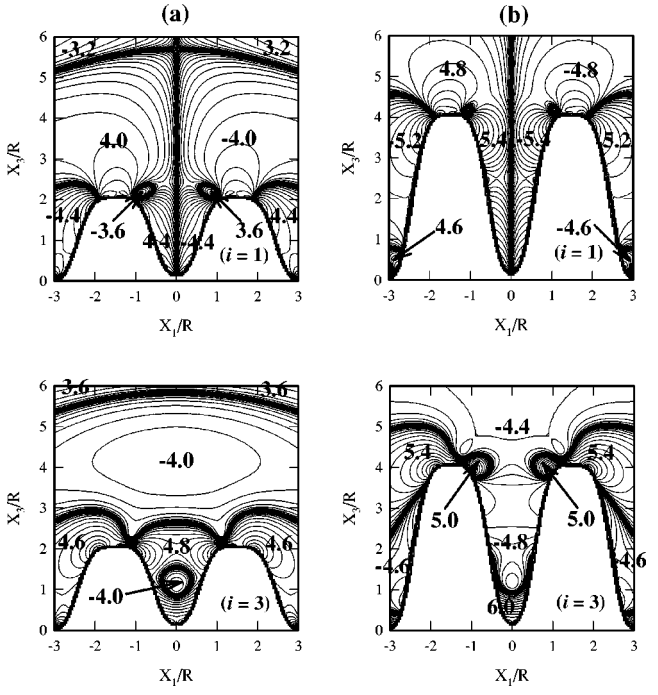

FIG. 4. Second-order pressure gradient field near a trench in the cases (a) $A=2R$, $\omega^*=0.56$, $\theta=0$ (left panel); and (b) $A=4R$, $\omega^*=0.38$, $\theta=0$ (right panel) given as contour maps of $\mathrm{sgn}(\boldsymbol{\nabla}_i\hat{p}^{(2)})/\log_{10}(|\nabla_i\hat{p}^{(2)}|)$ for $i=1$ and $i=3$. Thick lines correspond to zero gradients. A number with negative sign means that the gradient is oriented along the direction of the negative X_i's The number indicates the largest order of magnitude of the scaled gradient $\boldsymbol{\nabla}_i\hat{p}^{(2)}$. The interval between two successive isolines is equal to 0.2. Note the difference in order of magnitude between panels (a) and (b) due to the log scale.

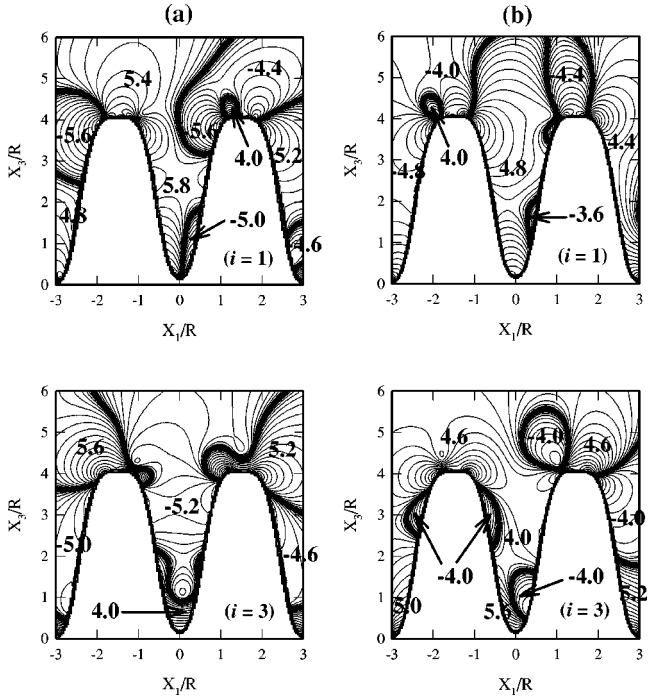

FIG. 5. Same as Fig. 4 but for (a) $A=4R$, $\theta\approx 90°$, $\omega^*=0.38$ (resonant mode); and (b) $A=4R$, $\theta\approx 90°$, $\omega^*=0.2$ (nonresonant mode).

IV. CONCLUSION

We have developed a theory of scattering of acoustic waves by supported ridges at a solid/liquid interface. This methodology enables us to calculate the first-order acoustic pressure amplitude (i.e., solution to the linear acoustic wave equation) as well as second-order corrections, solutions to the nonlinear Euler equation in the form of the time-independent gradients of the second-order acoustic pressure. Two systems are studied, namely, a single infinite rigid ridge and two parallel ridges (separated by a trench) supported by a rigid substrate in contact with a nonviscous fluid. The ridges have a exponential cross section and aspect ratios (height to width) of 1:1 and 2:1. We have calculated the vibrational density of states of these systems to identify frequencies at which resonances occur. At the resonant frequencies, the trenches exhibit noteworthy behaviors whereby the magnitude of the first-order acoustic pressure and the gradient of the second-order pressure take on significantly larger values compared to nonresonant conditions. The deepest trench (i.e., two ridges with the largest aspect ratio) studied shows the largest effect. The first-order pressure can become ten times larger than the amplitude of the incident wave in the confined space of the trench. A similar factor of 10 is also calculated for the magnitude of the second-order pressure gradient. The observed resonant behavior of a trench has interesting implications on the optimal conditions for cleaning integrated circuits using acoustic waves in water. In a previous study [3], we showed that a small spherical contaminant particle inside a trench is subjected in first approximation to an acoustic removal force proportional to the second-order pressure gradient. The gain of up to 1 order of magnitude in the value of the second-order pressure gradient upon tuning the acoustic wave frequency to that of a resonance of the trench will produce a comparable enhancement of the acoustic removal force on a contaminant particle. Excitation of resonant modes associated with a tenfold rise in the first-order pressure field inside a deep trench may lead to a pressure amplitude exceeding the cavitation threshold of the fluid. Nucleation of cavities in the confined space of a trench may provide sufficient energy concentration for effective removal of contaminant particles [13]. These optimal conditions may result in an increase in the efficiency of processes using acoustic waves for cleaning inside deep trenches. However current acoustic-based cleaning technologies use very low frequencies in comparison with those needed to stimulate resonances of submicron size trenches.

ACKNOWLEDGMENTS

This research was supported in part by a grant from the Center for Microcontamination Control at the University of Arizona. Three of us (A.K., Ph.L, and P.A.D.) would like to acknowledge the ''Laboratoire de Dynamique et Structures

des Matériaux Moléculaires,'' UFR de Physique, Université de Lille I, for its hospitality. The authors also acknowledge ''Le Centre de Ressources Informatiques'' (CRI) and ''Le Fond Européen de Développement Régional'' (FEDER) for providing some of the computer facilities. This work was also made possible partly thanks to the Convention 991/4269 FIRST-Europe (''Objectif 1'') from the Walloonia Region of Belgium and the European Union.

[1] S. Schwartzmann, A. Mayer, and W. Kern, RCA Rev. **46**, 81 (1985).
[2] P. A. Deymier, A. Khelif, J. O. Vasseur, B. Djafari-Rouhani, and S. Raghavan, J. Appl. Phys. **88**, 2423 (2000).
[3] P. A. Deymier, J. O. Vasseur, A. Khelif, B. Djafari-Rouhani, L. Dobrzynski, and S. Raghavan, J. Appl. Phys. **88**, 6821 (2000).
[4] H. Schlichting, *Boundary-Layer Theory*, 6th ed. (McGraw-Hill, New York, 1968).
[5] A. A. Maradudin, P. Ryan, and A. R. McGurn, Phys. Rev. B **38**, 3068 (1988).
[6] B. Djafari-Rouhani and A. A. Maradudin, Solid State Commun. **73**, 173 (1990).
[7] W. L. Nyborg, in *Acoustic Streaming*, *Physical Acoustics*, edited by W. P. Mason (Academic, London, 1965), Vol. II B, Chap. 11.
[8] L. Dobrzynski, Surf. Sci. Rep. **11**, 139 (1990).
[9] B. Djafari-Rouhani and L. Dobrzynski, J. Phys.: Condens. Matter **5**, 8177 (1993).
[10] A. Khelif and B. Djafari-Rouhani, J. Appl. Phys. **81**, 7141 (1997).
[11] A. Khelif, B. Djafari-Rouhani, and Ph. Lambin, Eur. Phys. J. B **21**, 437 (2001).
[12] B. Djafari-Rouhani, L. Dobrzynski, and A. Khelif, Prog. Surf. Sci. **48**, 301 (1995).
[13] R. Gouk, Masters thesis, University of Minnesota, 1996.